ADVANCED ENGINEERING MATERIALS
www.aem-journal.com

Design of Multiphase Compositionally Complex Alloys for Enhanced Hardness at Elevated Temperatures and Machinability: Comparative Study with Inconel 718

Laurent Peltier, Gaël Le Coz, Fodil Meraghni, and Jérome Slowensky*

Inconel 718 alloy is used for high-temperature industrial applications in its optimized multiphase metallurgical state. Nevertheless, the machining of Inconel 718 alloy becomes problematic and challenging. One alternative consists of developing a new material design strategy based on the metallurgy of high-entropy alloys (HEAs). These alloys have become a hotspot in the field of innovative high-temperature metallurgy toward the improvement of the alloy's manufacturability and thermomechanical properties. This study aims at designing, elaborating, and characterizing a new class of alloys with increased entropy, referred to as: "Inco-like." The mechanical responses of the alloys, in terms of hardness, have been analyzed using an indentation test at a wide range of temperatures. The dry machinability of the developed alloys has been performed and compared with that characterizing the Inconel 718 in terms of several machining features. Finally, the phases of the studied alloys have been analyzed using metallurgical investigations. The experimental findings and comparisons underscore the advantages of the high-entropy strategy in terms of tool wear reduction and cutting tool durability. The results demonstrate that the Inco-like HEA retains a significantly higher hardness of 291 Hv at 800 °C, compared to 160 Hv for Inconel 718 at the same temperature.

1. Introduction

Inconel alloys are extensively used in industry since the 1970s, especially in aeronautics and aerospace.[1–3] For these relevant industrial applications at high temperature, the Inconel 718 requires a structural hardening achieved through long heat treatment. The latter greatly improves the Inconel's performance at high temperatures and their good resistance to corrosion and oxidation. One of the most widely used alloys is Inconel 718, which is a nickel-based superalloy exhibiting relatively moderate entropy. However, machining Inconel is costly in terms of time and cutting equipment.[4] The use of the high entropy concept for the design of new alloys is attractive. In fact, these alloys do not necessarily require additional structural hardening, which implies a reduction of finishing processes. The objective of this study is to propose and validate the use of high entropy-based strategy to design a new class of alloys that exhibits enhanced thermomechanical properties and machinability than the Inconel alloys.

The high-entropy alloys (HEAs), compositionally complex alloys (CCAs), or multiprincipal element alloys (MPEAs) often have higher service temperatures than conventional low or medium-entropy alloys (MEAs).[5,6] Inconel class metals are multiphase alloys composed of a soft matrix, lava phases (30% harder than the matrix), and carbides (120% harder than the matrix).[7] This combination of soft and hard phases confers to the Inconel relevant mechanical performance at high temperatures due to the residual internal stresses. However, the Inconel has several drawbacks, which are induced by the properties contrast of its constitutive phases.[8] The hardness contrast between the matrix, the lava phases, and the carbides generally causes abnormal and excessive tool wear during the machining and finishing processes. In addition, it must be noted that the presence of hard phases in a soft matrix induces a low material removal rate and poor surface integrity. Furthermore, it should be mentioned that the annealing (ageing) treatment induces (γ) phase, which is reported by Zemzem et al.[9] At high concentrations, the (γ) phase may not necessarily enhance mechanical properties (Zemzemi et al.[9]). In contrast, when present in low amounts, the (γ) phase contributes to grain size refinement, thereby improving tensile properties and fatigue strength while maintaining good ductility, particularly under creep conditions. In addition, Zemzemi et al.[9] have shown that the carbide phases present particularly in the grain boundaries govern the evolution of the ductility and improve the high-temperature strength of the alloys. This aspect is particularly important in aerospace or nuclear applications needing a high level of reliability.

L. Peltier, G. Le Coz, F. Meraghni, J. Slowensky
LEM3
Arts et Métiers Institute of Technology
Université de Lorraine
CNRS
4 rue Augustin Fresnel, 57070 Metz, France
E-mail: laurent.peltier@ensam.eu

The ORCID identification number(s) for the author(s) of this article can be found under https://doi.org/10.1002/adem.202501146.

DOI: 10.1002/adem.202501146

The first quinary alloys have been developed and studied by Franz Karl Achart[10] in 1788. Since 2004, the study of the CoCrFeMnNi alloy[11,12] has the emergence of the concept of alloys with high entropy exhibiting innovative properties. Although these alloys are composed of at least five different elements, they can be in solid solution. This results in several effects: large lattice distortion,[13] cocktail effect,[14] and sluggish diffusion[15] in the alloy. HEAs have interesting thermomechanical properties, which are depending on the alloying elements, as shown by Jiao et al. in 2023.[16] The ability to incorporate multiple refractory elements into the same alloy increases the system's entropy and chemical complexity, offering intrinsic protection when exposed to high temperatures.[17,18] The enhanced hardness of high-entropy multiphase alloys, primarily attributed to lattice distortion and internal compressive stresses, serves as a foundation for developing new products, such as wear-resistant alloys[19–23] and materials that maintain high hardness at elevated temperatures.[14,24–29] The high-entropy strategy can be applied to families of alloys whose alloying elements allow phase changes, such as the martensitic transformation studied by Firstov et al. in 2014.[13,15,30–32] Despite the constant development of new HEAs, the literature dealing with the design of HEAs inspired by Inconel alloys remains limited if any. Specifically, for the machinability and finishing processes of the HEAs few studies have been published among them recent works dealing with the machining of the MEA or HEA.[33–36]

The primary focus of this article is the design and fabrication of novel compositionally complex alloys (CCAs) tailored for improved high-temperature hardness and enhanced machinability. With the focus of achieving lower manufacturing costs while maintaining comparable or improved machinability, the study presents a comparative evaluation between the developed CCAs and Inconel 718, in terms of key machinability-related properties, namely, wear resistance, high-temperature hardness, and surface roughness. It is worth noticing that the Inconel 718 is commonly used as a benchmark alloy for high-temperature applications.

Two new CCAs have been designed in this study. The first Inconel-like material is a MEA noted hereafter as: "Inco-like-M" whereas the second one is a HEA and referred to as "Inco-like-H."

The metallurgical and mechanical properties of Inco-like CCAs are compared with results obtained from the experiments performed on hardening commercial Inconel 718 alloy and/or those collected from the literature.[37–39] In this work, the Inconel 718 alloy was studied in its "As Received" metallurgical state. This state stands for an optimized configuration subsequent to annealing (ageing) treatment initially performed by the industrial partner. This configuration has been chosen to preserve the alloy's industrial conditions and thereby better highlights the benefits of the developed alloys. To avoid any misunderstanding, the term "As Received" will be replaced with "Optimized" (OP). Furthermore, it must be noticed that all the comparisons of the machining performances of the studied alloys deal with the case of finished machining operations. The hardness of the CCAs designed alloys has been analyzed using an indentation test at a wide range of temperatures (up to 800 °C). The machinability of the two alloys is investigated and compared in terms of surface quality and integrity as well as tool wear.[40,41]

The preparation and elaboration of the studied CCAs requires a multistep process. First, the alloying elements of the Inco-like alloys are identified. In the second step, the proportions of the elements will be optimized based on the high-entropy criteria for the metallurgy.[13,15,42–47] In the third step, the elaboration stage of these Inco-like alloys using a cold crucible will be detailed in the next section. The fourth step is devoted to the microscopic observations and characterization of these new alloys. A conclusion is drawn to highlight the main improvements and characteristics of these new alloys with respect to the Inconel 718.

2. Design and Characterization of New Produced CCAs

This section is aimed at investigating the two new alloys through an optimization of their chemical compositions with respect to the high-entropy criteria as well as their metallurgical structures analysis. It has been shown that mimicking the composition of the Inconel 718 leads to an improvement of the machinability features of the produced alloys.

2.1. Chemical Composition of the Studied Alloys

The Inconel 718 alloy is a nickel-based alloy, composed of 50% nickel, 20–26% of chromium, 20–23% of iron, 2.5% niobium, and 2.5% tantalum (at%). Molybdenum, titanium, aluminum, and other elements are present at very low content percentages. Niobium and tantalum are refractory elements. They confer to the CCA its mechanical properties at high temperatures. The increase in the proportion of these two elements improves the entropy of the mixture. The atomic radii of these two elements (on average 1.43) are much higher than those of the other three elements constituting the Inco-like alloy (on average 1.24). Consequently, the increase in the weight of these two elements causes a greater distortion of the crystal lattice than in Inconel 718 and thus induces internal stresses favorable to the structural hardening in the AC metallurgical state without heat treatment.

In addition, it is worth noting that to achieve a multiphase CCA, the Cr–Fe–Ni system was deliberately designed as a non-equiatomic alloy. Rather than adhering to conventional compositions, a less traditional formulation was explored to unlock new possibilities for optimizing both microstructure and properties. Specifically, increasing the chromium content is the most effective strategy to promote the formation of a chromium-rich phase while staying within the compositional domain of CCAs. This compositional shift also distinguishes the alloy from traditional Ni-rich Hastelloy-type and Fe-rich stainless steels, enabling the development of a material with distinct characteristics. Following the work of Wu et al. and Dong et al.[48,49] the Cr content was increased to improve high-temperature hardness and corrosion resistance. This approach intentionally prevents the design of an alloy such as $(CrFeNi)_{81}(NbTa)_{19}$, where CrFeNi is equiatomic.

Table 1 shows the compositions of the two studied alloys in comparison with that of the Inconel 718. In Inco-like alloys, the two elements Nb and Ta have the same proportion content

Table 1. Chemical composition and level entropy of the studied alloys (at%).

Alloys entropy level		Allaying elements [at%]					
		Ni	Cr	Fe	Nb	Ta	Others
Inconel 718	Low	50.0	22.0	22.0	2.0	2.0	2.0
Inco-like-M	Middle	30.0	35.0	25.0	5.0	5.0	0.0
Inco-like-H	High	23.0	32.0	26.0	9.5	9.5	0.0

compared to that in the Inconel 718. These two alloying elements are the most expensive and their proportions must be minimized to decrease the cost of the new HE alloys. Nevertheless, the chemical compositions have to be optimized to reach and verify the high entropy criteria. Zhou et al.[50] show that in the case of HEAs containing five elements, the content of the majority element cannot exceed 35% (at%). In the case of the studied high-entropy Inco-like alloys, the proportion of the Ni element is 30% for the Inco-like-M and 23% for the Inco-like-H (at%). The concentrations of the elements Cr and Fe in the composition of Inconel 718 are up to 20% (at%) whereas the composition of these elements (Cr and Fe) for the Inco-like alloys exceeds or equal to 33%. For the developed Inco-like alloys, the adopted compositions are as follows: $Cr_{32}Fe_{26}Ni_{23}Nb_{9.5}Ta_{9.5}$ (at%) for the Inco-like-H (high entropy) and $Cr_{35}Fe_{25}Ni_{30}Nb_5Ta_5$ (at%) for the Inco-like-M. One can notice that the proportions of Cr and Fe are similar for both studied Inco-like alloys. While the inclusion of Nb and Ta as alloying elements may be open to discussion, it is important to emphasize that these elements were selected for their refractory nature, which contributes to enhancing the high-temperature hardness of the developed alloys. Their concentrations were carefully optimized to balance performance with economic considerations, while maintaining the high-entropy design criterion $\Delta S_{mix}/R$ value of 1.50.

2.2. High-Entropy Criteria

The concept of HEAs has been introduced initially in the 1980s by Brian Cantor.[11,12] Subsequently, he developed the first HEA in 2004. The developed HEA was an equimolar solid solution alloy and was composed of five alloying elements, namely, CoCrFeMnNi. The author found a face-centered-cubic structure between these five different elements. However, a HEA must necessarily fit certain criteria to be considered as a HEA. These criteria were defined based on Cantor's alloy.

It has been stated by several authors, among them Zhang et al.[51] Guo et al.[52] Hasse et al.[53] and Yeh et al.[54] that the HEAs exhibit only one or two simple solid-solution phases, rather than chemically complex phases as for conventional alloys. In fact, for HEAs and according to thermodynamics, one can express the mixing Gibbs free energy as follows:

$$\Delta G_{mix} = \Delta H_{mix} - T\Delta S_{mix} \quad (1)$$

where ΔG_{mix} is the mixing of Gibbs free energy, ΔH_{mix} is the enthalpy of mixing, T is the temperature, and ΔS_{mix} is the variation of the entropy of mixing.

It is worth noticing that thermodynamically, an alloy tends to minimize its Gibbs free energy under the isobaric and isothermal conditions, and the mixing entropy evolves as a function of the number of alloying elements. It is expressed using Boltzmann law, as follows:

$$\Delta S_{mix} = -R * \sum_{i}^{n} c_i \ln(c_i) \quad (2)$$

where c_i stands for the molar concentration of the ith element and R is the universal gas constant ($R = 8{,}314\ J.K^{-1}.mol^{-1}$).

In their relevant works dealing with the monophase solid solution HEAs, Zhang et al.[56] proposed two criteria founded on the Hume–Rothery rules. The first one deals with the atomic size difference δ. This difference is expressed in percentage and stands for the difference of the atomic radii of the alloying elements composing a HEA:

$$\delta = 100\sqrt{\sum_{i=1}^{n} c_i\left(1 - r_i \Big/ \left(\sum_{i=1}^{n} c_i r_i\right)\right)^2} \quad (3)$$

where r_i is the atomic radius of the ith element and n is the number of the alloying elements.

The size differences induce lattice distortion in the crystal structure, which, in turn, affects the properties of the HEAs. It is important to note that a smaller δ value facilitates the incorporation of atoms into the crystal lattice, thereby increasing alloy solubility and reducing lattice distortion.

The second criterion is based on the estimation of the enthalpy of mixing derived from the Gibbs relationship:

$$\Delta H_{mix} = \sum_{i=1, j\neq 1}^{n} 4H_{mix}^{AB} * c_i c_j \quad (4)$$

The term $4H_{mix}^{AB}$ is the regular solid interaction parameter between ith and jth element and H_{mix}^{AB} is the enthalpy of mixing of the binary AB solid solution.

To predict and discriminate the formation of single-phase disordered solid solution, two additional criteria have also been introduced by Guo et al.[52] as well as Miracle et al.[57] founded on the rules of Hume–Rothery:

This electronegativity difference $\Delta\chi$:

$$\Delta\chi = 100\sqrt{\sum_{i=1}^{n} c_i\left(\chi_i - \left(\sum_{j=1}^{n} c_j\chi_j\right)\right)^2} \quad (5)$$

where χ_i and χ_j represent the Pauling electronegativity for the ith and jth elements, respectively.

The average of the valence electron concentration (VEC):

$$VEC = \sum_{i=1}^{n} c_i (VEC)_i \quad (6)$$

The limits of the thermodynamic criteria δ, ΔH_{mix}, χ and VEC, leading to a probable apparition of a solid solution multiphases, can be admitted as follows:[58]

$$\begin{aligned} &0\,\% < \delta < 4\,\%, \\ &-10\,\mathrm{kJ/mol} < \Delta H\mathrm{mix} < 10\,\mathrm{kJ/mol}, \\ &\chi \approx 0, \\ &6.87 < \mathrm{VEC} < 7.99 \end{aligned} \tag{7}$$

The main criterion is that the alloy must consist of at least five alloying elements whose proportions should be ranging between 5% and 35%.[11,50] The entropy of a HEA must also be high with a value of $(\Delta S_{\mathrm{mix}})/R > 1.5$, where R is the perfect gas constant. To avoid obtaining a highly distorted lattice and to enhance the appearance of several phases in the alloy, the criterion based on the difference in atomic radius between the atoms is verified.

This size parameter must be ranging between 4% and 8%.[43,59] Unlike the other publications related to the HEAs, where alloys must verify all the high entropy criteria, the new Inco-like alloys do not verify all these criteria because a single-phase solid solution is not desired or targeted. Indeed, Inconel 718 alloy is multiphase, and this aspect induces the high hardness properties of the Inconel and the Inco-like alloys. For this reason, the developed two HEAs are not single-phase to improve their hardness, which has been compared to that characterizing Inconel 718[6,22,60,61] and multiphase CCAs.[16,27,51,62–64] Therefore, the developed alloys are multiphase and consequently, the valence electron concentration VEC criterion[11,52] is comprised in the interval range of [6.87–7.99] for the HEAs that exhibit nonductile hard responses. The proportions of niobium and tantalum are limited due to their cost since they are expensive elements. Therefore, the respective content of these two alloying elements is minimized to obtain a value of $(\Delta S_{\mathrm{mix}})/R > 1.5$ required for the high entropy features. **Table 2** compares the results of the selected criteria for the development of high entropy multiphase alloys based on different alloys found in the literature.[11,13,15,24,40,47,55,56,62,65,66] It should be noted that the alloys developed by Zhang et al.[65] as well as those proposed by Lozinko et al.[62] and Jiao et al.[16] satisfy the same criteria as the Inco-like-H alloy.

3. Alloys Production and Characterization Methodologies

3.1. Materials Preparation Process

The five alloys studied in this work, namely, Fe_2Nb, CrFeNi, Cr_2FeNi, Inco-like-M, and Inco-like-H, have been produced by melting high-purity raw materials through a step-by-step process. It is worth noticing that the purity of the individual alloying elements exceeded 99.9 wt%. The alloys have been produced using a CFSYS cold crucible (or levitation furnace) coupled with a 50 kW FIVES induction furnace. The cold crucible is equipped with a laser pyrometer, which accurately measures the melting temperature (T_m) evolution of each alloy. Prior to heating, the cold crucible was evacuated 5 times to a vacuum pressure of 9×10^{-3} mbar and refilled with ultrapure argon gas to prevent contamination and oxidation. The melting process is then conducted under ultrapure argon at a pressure of 900 mbar. After each melting, the solidified ingot is manually flipped into the cold crucible. A total of ten melting cycles were performed to ensure thorough mixing of the elements in the alloy. The ingot is then cast into a square mold with a volume of 40 cm^3 (**Figure 1**).

Table 2. Criteria and validation values, in gray obtained values over the range of different criteria. The values of the table have been calculated using the equations 2 (ΔS_{mix}), 4 (ΔH_{mix}), 3 (δ), 5 (EN Pauling), and 6 (VEC).

Alloy compositions (at. %)			$\Delta S_{mix}/R$ x>1.5	ΔH_{mix} (kJ/mol) x≠[-10 ; 10]	δ (%) x>4	EN Pauling x≈0	VEC x∈[6.87 ; 7.99]
Inconel 718	[1-4, 7, 37-41, 68-69]		1.33 ☒	-9.66 ☒	3.98 ☒	0.13 ☑	8.33 ☒
$Co_{20}Cr_{20}Fe_{20}Mn_{20}Ni_{20}$	Cantor et al.	[11, 12]	1.61 ☑	-4.16 ☒	3.27 ☒	0.14 ☑	8.00 ☒
$Cr_{32}Fe_{26}Ni_{23}Nb_{9,5}Ta_{9,5}$	Inco-like-H	Present work	1.50 ☑	-12.79 ☑	5.64 ☑	0.13 ☑	7.25 ☑
$Cr_{35}Fe_{25}Ni_{30}Nb_5Ta_5$	Inco-like-M	Present work	1.37 ☒	-10.04 ☑	4.37 ☑	0.13 ☑	7.60 ☑
$(Ni_{27}Cu_{23})(Ti_{16}Hf_{19}Zr_{15})$	Peltier et al.	[13]	1.58 ☑	-29.08 ☑	10.71 ☑	0.27 ☒	7.23 ☑
$(Ti_{30}Hf_{19}Zr_{25})(NbTa)_{26}$	Peltier et al.	[15]	1.55 ☑	2.07 ☒	4.87 ☑	0.11 ☑	4.26 ☒
$Co_{22}Cr_{22}Fe_{22}Ni_{22}Nb_6Ta_6$	Jiao et al.	[16]	1.65 ☑	-11.84 ☑	6.75 ☑	0.16 ☑	7.76 ☑
$(NiCuPd)_{35}(TiHfZr)_{65}$	Piorunek et al.	[32]	1.74 ☑	-42.10 ☑	9.05 ☑	0.31 ☒	6.21 ☑
$Nb_{25}Ni_{25}Ta_{25}Ti_{25}$	Zhang et al.	[18]	1.38 ☒	-22.75 ☑	6.12 ☑	0.16 ☑	6.00 ☒
$Co_{25}Cr_{25}Fe_{25}Ni_{25}$	Moazzen et al.	[20]	1.38 ☒	-3.75 ☒	0.30 ☒	0.09 ☑	5.71 ☒
$Al_{5,9}Co_{23,5}Cr_{23,5}Fe_{23,5}Ni_{23,5}$	Hsu et al.	[24]	1.53 ☑	-6.75 ☒	3.48 ☒	0.10 ☑	7.94 ☑
$Hf_{20}Ta_{20}Ti_{20}V_{20}Zr_{20}$	Pole et al.	[26]	1.61 ☑	-0.32 ☒	7.06 ☑	0.12 ☑	4.4 ☒
$Ta_{20}Ti_{20}V_{20}W_{20}Zr_{20}$	Pole et al.	[26]	1.61 ☑	-4.16 ☒	6.80 ☑	0.35 ☒	4.8 ☒
$Al_{19}Cr_{27}Fe_{27}Ni_{27}$	Cui et al.	[27]	1.38 ☒	-11.74 ☑	5.72 ☑	0.12 ☑	7.05 ☑
$Al_{20}Co_{20}Cu_{20}Fe_{20}Ni_{20}$	Guo et al.	[34-35, 50]	1.61 ☑	-5.28 ☒	5.61 ☑	0.11 ☑	8.20 ☒
$Cu_{29}Fe_{11}Ni_{29}Mn_{20}V_{11}$	Peltier et al.	[47]	1.52 ☑	-0.26 ☒	3.13 ☒	0.15 ☑	8.92 ☒
$Co_{25}Cr_{17}Fe_{17}Ni_{25}Ti_{17}$	Zhang et al.	[55-56]	1.59 ☑	-15.61 ☑	6.25 ☑	0.14 ☑	7.75 ☑
$Al_{16,4}Co_{16,4}Cr_{16,4}Fe_{16,4}Ni_{34,4}$	Lozinko et al.	[62]	1.55 ☑	-11.94 ☑	5.38 ☑	0.12 ☑	7.70 ☑
$Co_{20}Cr_{20}Cu_{20}Fe_{20}Ni_{20}$	Verma et al.	[66]	1.61 ☑	3.20 ☒	1.03 ☒	0.09 ☑	8.80 ☒

Criteria chosen to promote the formation of multiphase HEA.

☒ Criterion not validated
☑ Criterion validated
➡ Alloys that validate all the criteria

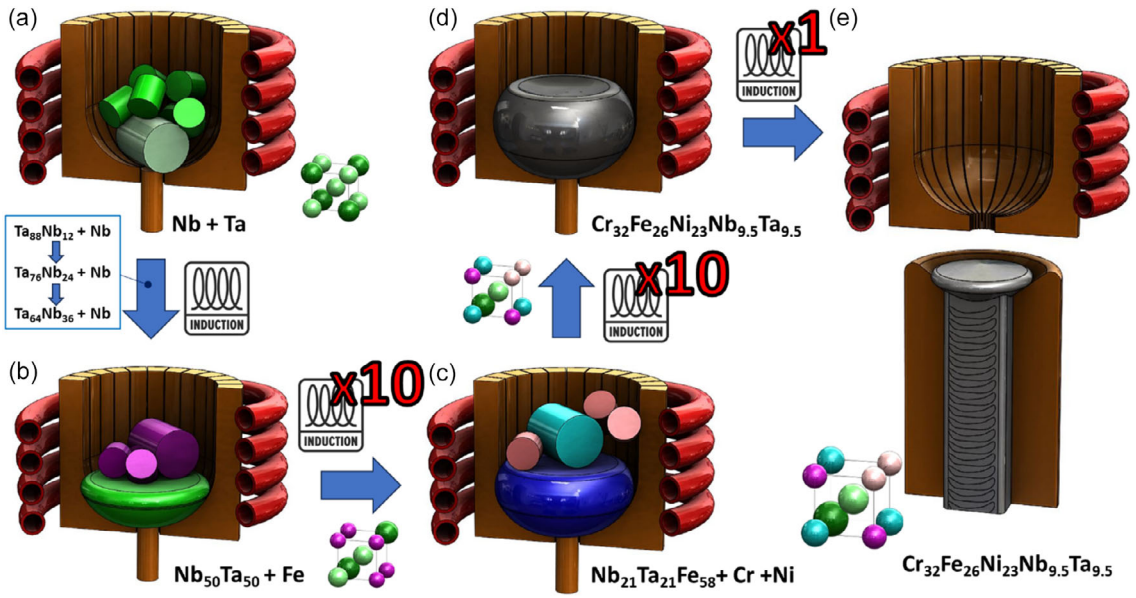

Figure 1. Schematic drawing showing the five steps of the metallurgical preparation of high-entropy Inco-like-H alloy. These steps are organized as follows: a) progressive production of master alloy #1 in four stages where the Nb is added progressively, leading to b) the production of master alloy #2 (NbTaFe) in a single stage, then the step c) corresponding to the melting of the previous alloy with chromium and nickel, in the step d) the final alloy is produced in a single stage after several melting using an induction furnace. Finally, the ingot molding is achieved to obtain the final alloy in its "As Cast" or AC metallurgical state, as illustrated in e).

The CCAs have been produced by mixing five pure elements: Ni, Cr, Fe, Nb, and Ta in a cold crucible. The magnetic fields allow the fusion of the elements, the levitation of the batch and the mixing of the elements in the liquid bath. The alloying elements employed for the developed two Inco-like alloys (with high and medium entropy) have different melting temperatures. Hence, the melting temperature of refractory elements is higher than that characterizing other transition metals. In addition, the melting temperature of tantalum (3020 °C) is higher than the evaporation temperature of chromium (2672 °C). To prepare the alloy without element loss during the melting of tantalum, the alloys have been prepared incrementally in several steps and by using master alloys. Indeed, mixing progressively the Niobium element in the Tantalum element makes it possible to lower progressively the melting temperature of the binary alloy TaNb below the evaporation temperature of Chromium. Thus, the risk of chromium evaporation is limited, and the initially chosen compositions of Inco-like-M and Inco-like-H alloys are then maintained.

The production of these two Inco-like alloys is done using a cold crucible. The progressive production of the master alloy $Nb_{50}Ta_{50}$ with a melting temperature of less than 2700 °C is made incrementally in four steps where the Ta content is decreased progressively: 90% of tantalum, 75%, 65%, and then finally 50% (at%) (Figure 1a). The advantage of using a master alloy $Nb_{50}Ta_{50}$ produced progressively is to have an alloy whose melting temperature is lower than the boiling temperature of the three other elements ($T_B^{Cr} = 2672$ °C, $T_B^{Fe} = 2750$ °C, and $T_B^{Ni} = 2732$ °C). The second master alloy with three elements is $Nb_{21}Ta_{21}Fe_{58}$ (Figure 1b,c), it results from the addition of the entire quantity of Fe proportion to the first master binary alloy TaNb. The end of the casting process corresponds to the addition of chromium and nickel fillers and the second master ternary alloy NbTaFe. One obtains hence the high and MEAs referred to as Inco-like-H and Inco-like-M, respectively.

It should be noted that the produced ingots were neither homogenized nor solution-treated after casting. In addition, two metallurgical states were considered for further characterizations: the first one noted hereafter "As-Cast" (AC) just after melting for Fe_2Nb, CrFeNi, Cr_2FeNi, Inco-like-H, and Inco-like-M. The second one for the commercial Inconel 718 alloy noted hereafter "Optimized" (OP).

3.2. Metallurgical Analysis Procedures

The metallurgical characterization of the three studied alloys (Inco-like-M, Inco-like-H, and Inconel 718) has been achieved according to two main steps: microstructural investigation and the characterization of the chemical composition of each alloy. The microstructure observations have been performed using a Zeiss Supra 40 field emission gun scanning electron microscope (SEM). The chemical composition of the samples studied has been analyzed by EDX (energy-dispersive X-ray spectrometry). The crystallographic phases have been identified and analyzed through Rigaku X-ray diffraction (XRD) using Cu-Ka radiation at room temperature. The XRD analysis has been performed before and after heat treatment according to XRD powder mode using an accelerating voltage of 40 kV and an intensity of 30 mA. The diffractograms have been indexed with suitable softwares (Maud and CaRIne) that allowed the determination of the crystallographic structures and their lattice parameters.

3.3. Mechanical Testing Methods

A mechanical macrohardness tester (indenter) has been utilized to determine the hardness of the three alloys in a wide range of temperatures (from 25 to 800 °C). The macroindentation load has been set at 30 N and the tests have been repeated three times for each temperature and each alloy. The indentation test device has been modified to reach an operating temperature of up to 800 °C. To this end, a heating plate controlled by an optical pyrometer ensures the heating of the sample, which is positioned in an insulating enclosure during the test. The length of the indenter setup has been modified for hot testing, and the hardness measurements were carried out once the sample had completely cooled. This test bench is detailed in **Figure 2**.

3.4. Machinability Analysis Procedures

For the three studied alloys, the cutting operations have been performed on a Roeders RXP200DS 5 axes high-speed machining center (3000–60 000 rpm). The selected cutting tools are solid micro grain tungsten carbide (WC) with a 4 mm diameter, two flute ball nose end mills with a helix angle of 30°, and a nanocoating AlCrN (3200 Hv). The machining conditions are identical for the 3 alloys studied, Inconel 718, Inco-like-M and Inco-like-H respectively, and are summarized in **Table 3** and the test bench is detailed in **Figure 3**.

The Flank wear (V_b) has been repeatedly measured with a Tesa Visio microscope having digital micrometer heads. Workpiece surfaces are observed with a Leica DCM3D allowing hence to extract the surface roughness (R_a) for both new and worn cutting tools that have been taken parallel to the feed direction. The performed machining tests are finish-milling operations with fixed operating parameters that involve a maximum peripheral cutting speed of 45 m/min, a feed per tooth of 0.080 mm, and a stepover depth of cut of 0.1 mm. The cutting conditions are appropriate for a finish-machining regime. All machining trials have been performed in down milling and dry conditions. According to Kim et al.[67] a horizontal downward orientation with the workpiece inclined/tilted at 45° is chosen to lead to a cutting speed variation along the tool-workpiece contact region from 45% to 89% of the programmed diameter speed. The cutting length for each pass depends on the 20 mm width of the sample. It must be noted that between each pass, an offset of 0.5 mm is set.

Table 3. Machining conditions for the alloys studied Inconel 718, Inco-like-M, and Inco-like-H.

Parameters		
Cutting speed	V_c [m min^{-1}]	45
Feed	f [mm th^{-1}]	0.08
Depth of cut	a_p [mm]	0.1
Offset	a_e [mm]	0.5
Inclinaison angle	τ [°]	45
Tool diameter	∅ [mm]	4

4. Results and Discussions

4.1. Characterization of the Structures

Figure 4a–c shows the three studied alloys under the SEM investigation; one can observe that Inco-like-H (Figure 4c) is multiphase as Inconel 718 alloy (Figure 4a). Different phases can be noticed in the Inconel 718 alloy like metallic carbides or lava phases with high hardness.[68,69] It must be mentioned that these metallic phases make Inconel 718 alloy difficult to machine and induce more wear to the cutting tools, reducing hence their durability.

Like the HEAs studied by Zhang et al.[65] as well as those investigated by Lozinko et al.[62] the developed Inco-like-H is composed of three distinct phases (**Figure 5**). In this figure, one can notice that the Inco-like-H exhibits several phases, whose averaged chemical compositions have been measured using EDX mapping: 1) a light gray phase with high entropy composition $Cr_{28}Fe_{24}Ni_{20}Nb_{14}Ta_{14}$ corresponding to $\Delta S_{mix}/R = 1.57$, 2) a dark gray phase with low entropy composition $Cr_{50}Fe_{27}Ni_{23}$ ($\Delta S_{mix}/R = 1.04$), and 3) a medium entropy eutectic $Cr_{34}Fe_{27}Ni_{35}Nb_2Ta_2$ ($\Delta S_{mix}/R = 1.24$). The dark phase ($Cr_{50}Fe_{27}Ni_{23}$) is

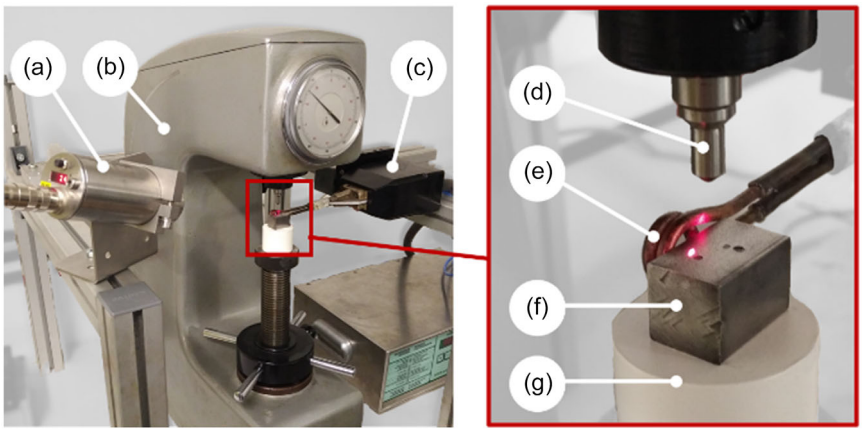

Figure 2. Temperature hardness test bench including different components: a) temperature measurement by laser pyrometer, b) mechanical hardness tester, c) induction heater, d) indenter, e) inductor, f) alloy sample, and g) thermal insulator.

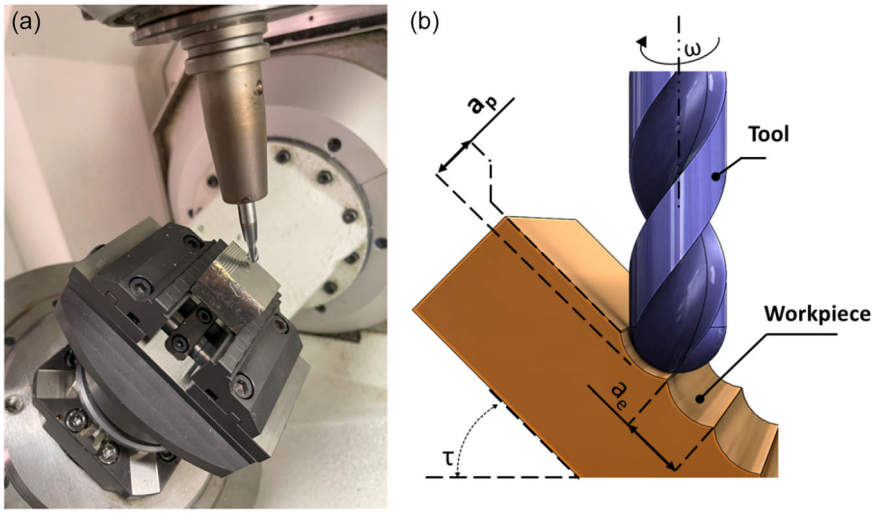

Figure 3. Experimental setup for optimal milling experiments on a 5-axis machining center: a) overview and b) schematic for cutting conditions and tool tilting.

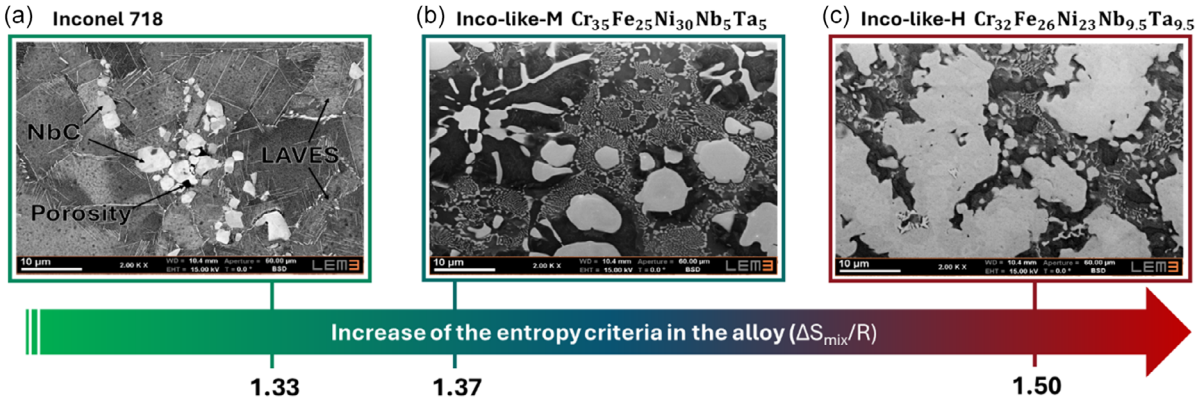

Figure 4. SEM observations of the studied alloys characterized a multiphase structure and increasing (ΔS_{mix})/R values: a) Inconel 718 alloy, b) Inco-like-M alloy, and c) Inco-like-H alloy.

very close to the ternary alloy Cr_2FeNi in terms of chemical composition.

It should be mentioned that in the case of cooling for both developed CCAs, solidification from the liquid phase does not induce any lava phases, as the multiphases present in the "As-Cast" state, although different, are still chemically similar, as illustrated in Figure 4 and 5.

The SEM observations in Figure 4, 5 were conducted at the same magnification; a meaningful qualitative comparison is possible. In fact, it is evident that the light gray phase, identified as a high-entropy $Cr_{28}Fe_{24}Ni_{20}Nb_{14}Ta_{14}$ phase, is more prevalent in Inco-like-H (Figure 5d and Figure 4c) than in Inco-like-M (Figure 4b). On can also notice that the Inco-like-M exhibits more eutectic phase with middle entropy ($Cr_{34}Fe_{27}Ni_{35}Nb_2Ta_2$) compared to Inco-like-H.

For the sake of completeness and comparison of the diffractogram peaks of the Inco-like-H alloy using XRD, three supplementary alloys have been produced using the cold crucible and studied via XRD and SEM, as shown in **Figure 6**: the ternary $Cr_{50}Fe_{27}Ni_{23}$ alloy (similarly to Cr_2FeNi), the quinary $Cr_{28}Fe_{24}Ni_{20}Nb_{14}Ta_{14}$ alloy (similarly to Fe_2Nb) and the quinary $Cr_{34}Fe_{27}Fe_{35}Nb_2Ta_2$ alloy (similarly to Fe_2Nb).

Figure 6 shows the different diffractograms over a 2θ angle range of 30°–70°of the phases and alloys studied. The diffractogram of the Inco-like-H alloy shown in Figure 6 has been enriched by the other diffractograms characterizing the different phases highlighted during the chemical analysis. Figure 6 is the superposition of all the XRD peaks of the different phases observed in the Inco-like-H alloy. Using CaRIne software,[66,70,71] the diffractions of alloys are established in the literature making possible the identification of the structures of the phases present in the developed alloys. The green curve (Figure 6d) corresponds to the diffraction of the Fe_2Nb alloy, exhibiting five peaks located at 38.4°, 42.0°, 44.8°, 45.5°, and 47.7°. The red curve (Figure 6c) represents the diffractogram of the CrFeNi alloy, with three peaks observed at 45.6°, 46.0°, and 66.1°. The blue curve (Figure 6b) corresponds to the Cr_2FeNi alloy, displaying two peaks located at 44.9° and 52.5°.

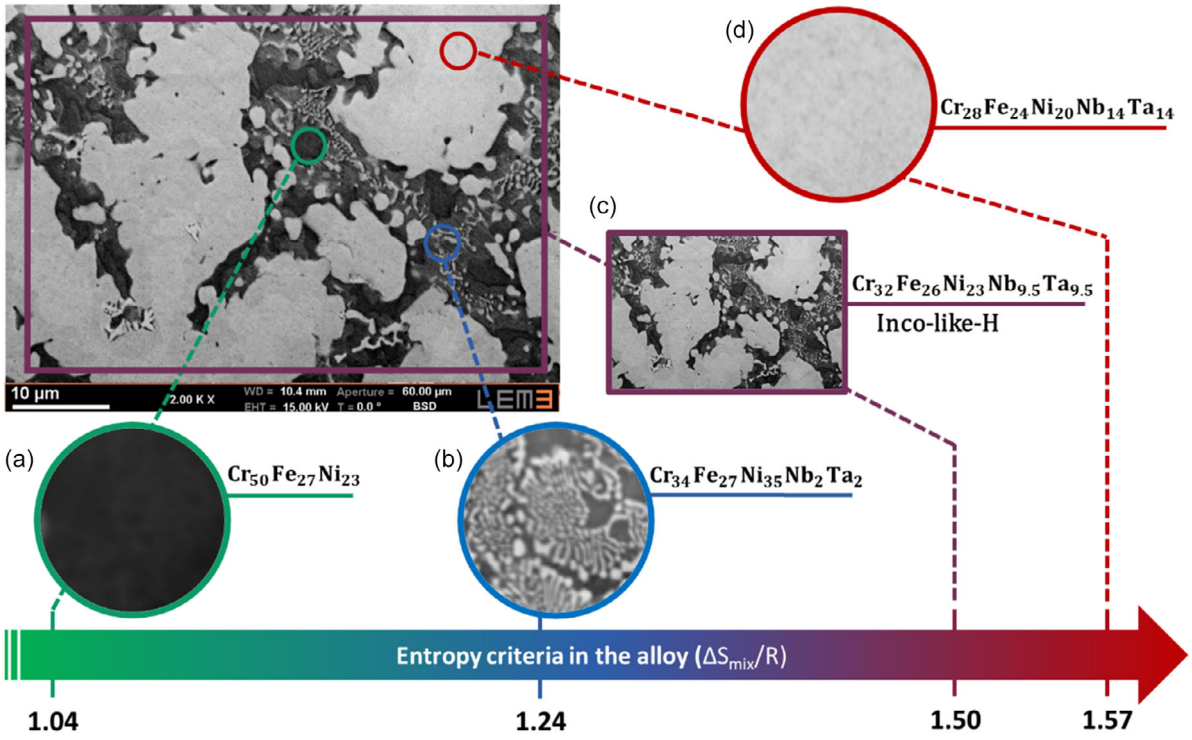

Figure 5. SEM observations and chemical compositions (at%) of the studied phases of the Inco-like-H alloy: a) a dark gray phase with low entropy $Cr_{50}Fe_{27}Ni_{23}$, b) a eutectic with middle entropy $Cr_{34}Fe_{27}Ni_{35}Nb_2Ta_2$, c) the studied alloy with high entropy $Cr_{32}Fe_{26}Ni_{23}Nb_{9.5}Ta_{9.5}$, and d) a light gray phase with high entropy $Cr_{28}Fe_{24}Ni_{20}Nb_{14}Ta_{14}$.

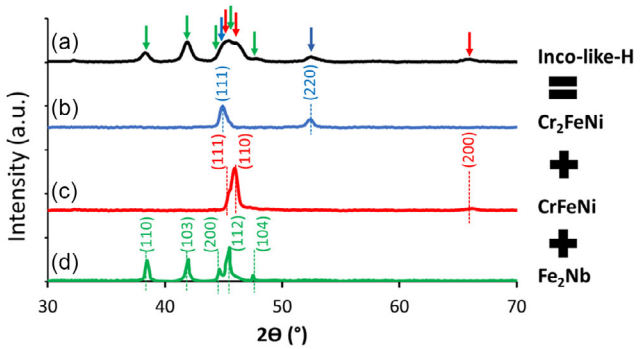

Figure 6. Diffractogram results of the multiphase studied Inco-like-H alloy: a) in black, Inco-like-H alloy, b) in blue, Cr_2FeNi alloy, c) in red, CrFeNi alloy produced in the present work and studied in ref. [73], and d) in green, Fe_2Nb alloy produced in the present work and studied in.[74]

The CrFeNi phase has a cubic-centered (CC) structure and the Cr_2FeNi phase has a face-centered cubic (CFC) structure. The Fe_2Nb phase fits well with the curves with a hexagonal structure, which allows assigning its structure parameters to those of one of the alloy phases.

4.2. Hardness Test

First, the hardness of Inconel 718 was measured over a wide range of operating temperatures. These measurements were conducted to demonstrate that Inconel 718, used as the reference alloy for comparison with the two developed Inco-like HEAs, exhibits a hardness evolution similar to that reported in the literature. It is evident that the hardness of Inconel 718 as a function of temperature follows the same trend observed by several authors, as shown in **Figure 7**a. This consistency supports the validity of our findings and highlights the added value of the newly developed HEAs in terms of hardness, as depicted in Figure 7b.

In this study, the results shown in Figure 7b confirm that the Inco-like-H alloy has a higher hardness than Inconel 718 and the Inco-like-M alloys over the entire tested temperature range. One can notice that the Inco-like-H alloy maintains a hardness level of 291 Hv at 800 °C compared to the level of 191 Hv for the Inconel 718 alloy, whereas the Inco-like-M alloy has a value of 218 Hv at this temperature. It is easy to compare the hardness of these three alloys for different operating temperatures. Indeed, the Inconel 718 alloy has a hardness close to 300 Hv at 500 °C while the MEA reaches this hardness level at 600 °C. This hardness of 300 Hv is observed on the HEA at 800 °C, which corresponds to an operating temperature 300 °C higher than that of the reference alloy, Inconel 718. This is an important result, as it confirms that Inco-like alloys offer a higher level of hardness than Inconel 718 over a wide temperature range.

4.3. Cutting Tool Flank Wear

To compete effectively with the Inconel 718 alloy, the new Inco-like alloy with high entropy must be easier to machine, reducing

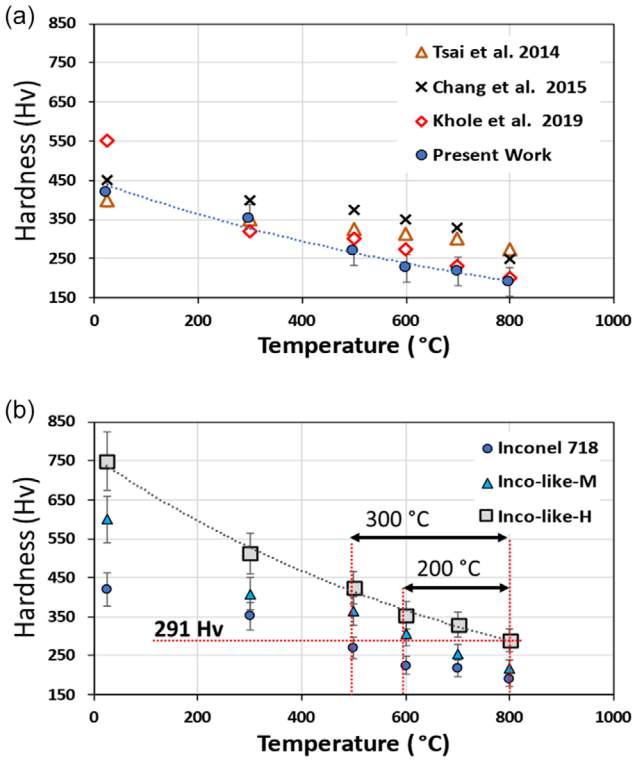

Figure 7. Hardness results (Hv) between 25 °C and 800 °C: a) Vickers hardness of Inconel 718 alloy from the scientific literature and those of this study and b) comparison of the Vickers hardness tests in the present work.

hence the manufacturing process costs. Several grooves are machined to achieve substantial tool wear. The tests are stopped when a clearance wear (V_b) of the order of 0.1 mm is reached. This value corresponds to a significant degradation of the cutting edge when machining Inconel 718 with a 4 mm diameter cutting tool. The evolution of the V_b value as a function of the cumulative machined length is shown in **Figure 8**. The machining of Inconel 718 is characterized by a rapid increase in the V_b values from the beginning of machining to a working length of 1.8 m. A pseudo plateau is reached and then an increase in wear occurs above 5 m. The test is interrupted at 7 m with a V_b value of 0.1 mm.

Figure 8a shows apparent wear resulting from the taper contact on the flank face. The work-hardening capacity of Inconel induces this wear pattern, which is well known in the literature.[41] Welding and adhesion on the cutting tool occur to a chip adhered to the cutting face, to form a built-up edge (BUE). This observation reveals a high-temperature level reached during the chip formation. As the BUE is regularly renewed, the tool coating is quickly removed, and the cutting edge is weakened. The latter is amplified by a continuous abrasion all along the cutting edge and a localized notch wear potentially occurs. However, the tests are not carried out to the point of edge breakdown as Kaynak et al.[72] The flank wear exhibited by the Inco-like-M is characterized by continuous evolution until a machine length up to 5 m then one can notice a reduced evolution followed by a rapid increase beyond a machined length of 7 m. In the running-in phase, the wear is lower than that exhibited by the Inconel 718. However, after 5 m, the clearance wear values are equivalent to those measured on the Inconel 718. For Inco-like-H, the running-in phase is equivalent to Inconel 718 but with a similar

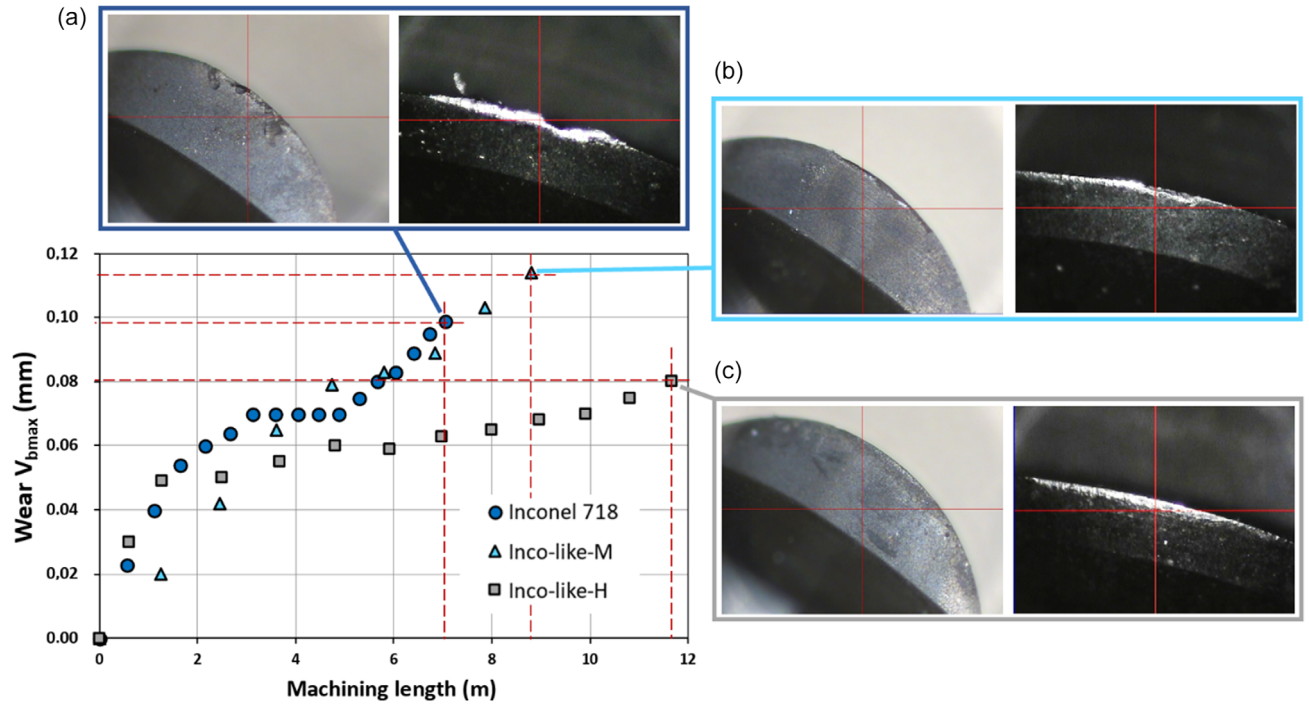

Figure 8. Measurement of the wear V_b (mm) of the milling cutter and plotted as a function of the cumulative machined length (m) and cutting edges at the end of machining at 7, 9, and 12 m respectively for: a) Inconel 718, b) Inco-like-M, and c) Inco-like-H.

slope concerning the cumulative machine length. One can notice that only after 1 m machining, a pseudo-plateau is reached with a stabilized evolution of wear until a length up to 12 m corresponding to a V_b of about 0.08 mm. The test is interrupted after 12 m of machining with a draft wear close to that observed on the Inconel but without any bonding nor BUE observations, Figure 8c.

4.4. Surface Roughness

The degradation of cutting tools leads to a gradual deterioration of the surface finish during machining operations. Among the relevant key indicators for monitoring this a progressive deterioration of the surfaces, the evolution of their roughness (R_a) measured at the bottom of the machined groove along the cutting direction. **Figure 9** illustrates the evolution of (R_a) as a function of the accumulated cutting length, for the three studied alloys. As illustrated in Figure 9, there is a clear trend indicating that surface roughness increases progressively with machining length. One can notice that this effect is particularly pronounced during the machining of Inconel 718. For this alloy, the R_a value begins at ≈1 µm for the first groove and increases progressively, reaching up to 3.2 µm by the end of the test corresponding to a machining length of 7 m. The increase in surface roughness is attributed to several factors such as tool wear, which become more significant over longer machining distances as shown in **Figure 10**.

This significant rise in roughness correlates strongly with the accelerated wear mechanisms affecting the cutting edge, including flank wear, notch wear, and the formation of a BUE. These phenomena contribute to surface irregularities, and in some cases, the adherence and subsequent deposition of material fragments onto the workpiece surface—as shown in Figure 10a—further degrade the surface finish. These findings highlight the challenges associated with maintaining surface quality in prolonged machining operations involving difficult-to-machine materials like Inconel 718.

In the case of notch wear, the geometry of the tool's cutting edge undergoes considerable alteration, leading to irregularities in the surface topography. However, due to the overlap strategy implemented during machining—where each subsequent pass

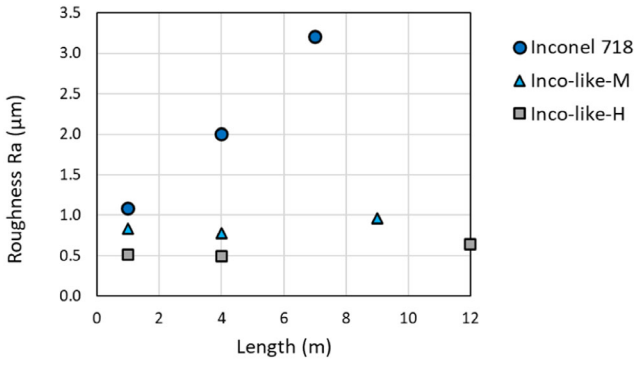

Figure 9. Evolution of the roughness R_a (µm) at the bottom of the grooves for the three studied alloys. A clear trend shows that surface roughness increases progressively with machining length, particularly pronounced for Inconel 718 whose R_a increases rapidly from 1 µm for the first groove and reaches 3.2 µm for a machining length of 7 m.

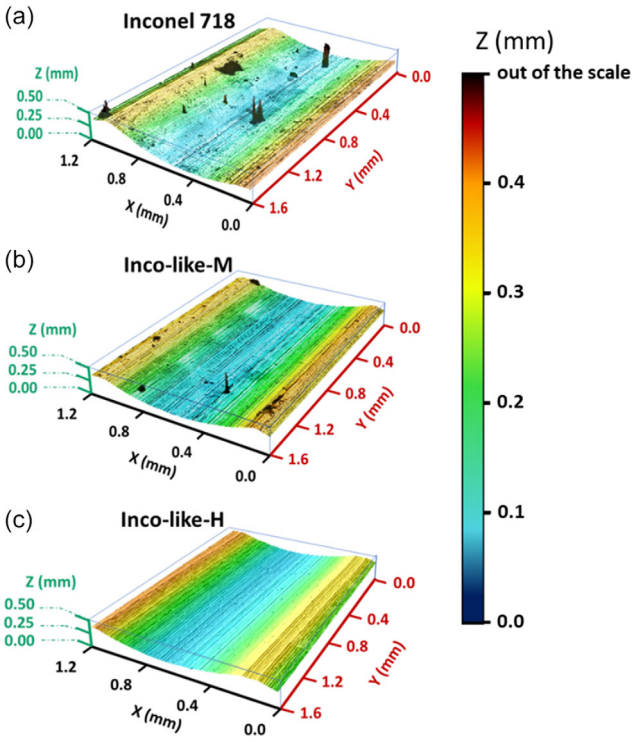

Figure 10. Surfaces at the end of the tests observed with Leica: a) Inconel 718 alloy, b) Inco-like-M alloy, and c) Inco-like-H alloy.

overlaps the previous groove by 0.5 mm, as described in Section 3.4—these locally damaged areas are remachined and effectively eliminated, minimizing their impact on the final surface condition. Concerning the formation of a BUE, fragments are removed during the formation of the new surface, and they cover the machined surface leading to a degradation of the sample's surface.[40]

In contrast, the machining of CCAs, such as Inco-like-M and Inco-like-H, results in consistently lower surface roughness values. Throughout the entire test, R_a remains below 1 µm and exhibits a stable, gradual evolution with respect to the machining length reaching 12 m for the Inco-like-H. The investigation of the machined surfaces in Figure 10b and c reveals a notably different wear pattern compared to Inconel 718. Particularly, for the Inco-like-H, the surfaces display fine, uniform lines aligned with the feed direction of the tool, which are indicative of minimal tool wear and correspond to the microgeometry of the tool's cutting edge. These subtle tool marks suggest that wear is limited primarily to minor abrasive effects rather than more severe forms of defects. Furthermore, the absence of debris or smeared material residues on CCA-machined surfaces highlights a key advantage: the suppression of BUE formation. Because CCA materials do not promote the accumulation of BUE on the cutting face, the resulting surface finish remains clean and homogeneous, thus preserving the integrity and dimensional accuracy of the machined component. This improved surface quality has critical implications for applications where fatigue resistance, thermal stability, and surface integrity are of paramount importance.

5. Main Outcomes and Essential Takeaways from the Study

This study compares the mechanical properties (hardness and machinability) of three alloys: 1) Inconel 718, a well-known low-entropy alloy, 2) a MEA called Inco-like-M ($Cr_{35}Fe_{25}Ni_{30}Nb_5Ta_5$), and 3) a HEA called Inco-like-H ($Cr_{32}Fe_{26}Ni_{23}Nb_{9.5}Ta_{9.5}$). The latter two were specifically designed for this work. In designing Inco-like-M and Inco-like-H, all criteria for forming multiphase alloys were met. Unlike traditional single-phase HEA design, this study uses different target values for VEC and δ. Inco-like-M meets all the proposed CCAs criteria except for the entropy threshold ($\Delta S_{mix}/R = 1.37 < 1.5$), and serves as a comparison baseline. Inco-like-H, however, satisfies all high-entropy criteria and exhibits a multiphase structure similar to Inconel 718. The benefits of CCAs without precipitates were explored across temperature ranges. Hardness tests show that Inco-like-H maintains superior Vickers hardness compared to Inconel 718 from 25 to 800 °C (e.g., 291 Hv vs 160 Hv at 800 °C). Tool wear and machinability were also assessed, with Inco-like-H reducing tool wear by ≈40% and achieving better surface finishes (roughness < 0.5 μm vs up to 3.2 μm for Inconel 718 after 8 m of machining). However, Inco-like-H is more costly due to its higher Nb and Ta content. Inco-like-M, while meeting most criteria, shows no significant mechanical advantage over Inconel 718. Notably, Inco-like-H can be used in the "As-Cast" state without the need for additional structural hardening, unlike Inconel 718. This reduces processing costs and makes it a suitable candidate for additive manufacturing after atomization. In summary, the developed CCAs outperforms Inconel 718 in hardness and machinability and shows strong potential for high-temperature applications. Future work will investigate a naturally formed single-phase alloy ($Cr_{28}Fe_{24}Ni_{20}Nb_{14}Ta_{14}$), comparing it to Inco-like-H to confirm the role of structural hardening in performance improvements. The results highlight the promise of Inco-like alloys in improving manufacturing efficiency and reducing tool wear, opening avenues for further CCAs or MPEAs development.

6. Concluding Remarks

This study compares the mechanical properties, hardness and machinability, of three alloys: the industrial LEA Inconel 718, a MEA named Inco-like-M ($Cr_{35}Fe_{25}Ni_{30}Nb_5Ta_5$), and a HEA named Inco-like-H ($Cr_{32}Fe_{26}Ni_{23}Nb_{9.5}Ta_{9.5}$). The two Inco-like alloys are specially developed for this research. Inco-like-H is designed to meet all high-entropy criteria, including a multiphase structure, while Inco-like-M, with a slightly lower entropy value ($\Delta S_{mix}/R = 1.37$), serves as a reference point. The analysis and the comparison of the experimental results obtained lead to the following concluding remarks: Inco-like-H shows higher hardness, maintaining 291 Hv at 800 °C compared to 160 Hv for Inconel 718. Inco-like-H demonstrates 40% less tool wear and improved surface finish (roughness < 0.5 μm vs 3.2 μm for Inconel 718). Although more expensive due to higher Nb and Ta content, Inco-like-H and Inco-like-M can be used without heat treatment, lowering processing costs. Inco-like-H and Inco-like-M are suitable for additive manufacturing due to their intrinsic mechanical properties achieved in the "As-Cast" state and their high melting point (1600 °C). Inco-like-H exhibits superior mechanical performances compared to Inco-like-M.

The study confirms that the performances of the developed Inco-like-H are induced by a combined effects of structural hardening and alloying elements (composition). Future work is suggested on a naturally formed single-phase alloy ($Cr_{28}Fe_{24}Ni_{20}Nb_{14}Ta_{14}$) to further validate this.

Overall, Inco-like-H shows strong potential as a next-generation high-temperature alloy, offering enhanced mechanical performance and manufacturing efficiency compared to traditional solutions.

Acknowledgements

The authors would like to thank the colleagues who run the experimental facilities platforms "Procédés," "MicroMat," and "MécaRhéo" and the intensive computing platform "Cassiopée" at the Ecole Nationale Supérieure d'Arts et Métiers. The authors would like to thank our students Cyril Antony, Valentin Heyer, and Loic Klein for their help, which greatly facilitated this study. This paper is dedicated to the memory of our colleague Lionel Schivre who died unfortunately before publication.

Conflict of Interest

The authors declare no conflict of interest.

Data Availability Statement

Data sharing is not applicable to this article as no new data were created or analyzed in this study.

Keywords

high-entropy alloys, hot-temperature hardness, Inconel 718, machinability, multiprincipal element alloys

Received: April 28, 2025
Revised: July 7, 2025
Published online:

[1] E. Hosseini, V. A. Popovich, *Addit. Manuf.* **2019**, *30*, 100877.
[2] S. Pratheesh Kumar, S. Elangovan, R. Mohanraj, J. R. Ramakrishna, *Mater. Today Proc.* **2021**, *46*, 7892.
[3] G. A. Knorovsky, M. J. Cieslak, T. J. Headley, A. D. Romig, W. F. Hammetter, *Metall. Trans. A* **1989**, *20*, 2149.
[4] G. Mustafa, M. T. Anwar, A. Ahmed, M. Nawaz, T. Rasheed, *Adv. Eng. Mater.* **2022**, *24*, 2200202.
[5] K. Praveen, *Adv. Eng. Mater.* **2018**, *20*, 1700645.
[6] K. Tsao Yeh, *Adv. Eng. Mater.* **2017**, *19*, 1600475.
[7] W. Wang, C. Zhu, J. Zeng, C. Lu, H. Qian, H. Xu, P. Lyu, *Mater. Sci.* **2020**, *51*, 2306.
[8] I. A. Choudhury, M. A. El-Baradie, *J. Mater. Proc. Technol.* **1998**, *300*, 278.
[9] F. Zemzemi, J. Rech, P. Kapsa, A. Dogui, **2006**.
[10] A. Franz Karl, *Rec. Prop. Alliag. Métall.* **1788**.
[11] B. Cantor, I. T. H. Chang, P. Knight, A. J. B. Vincent, *Mater. Sci. Eng. A* **2004**, *375*, 213.
[12] B. Cantor, *Prog. Mater. Sci.* **2020**, *120*, 100754.

[13] L. Peltier, P. Lohmuller, F. Meraghni, S. Berveiller, E. Pattor, *Shape Memory Superelas.* **2020**, *6*, 273.
[14] J. Chen, X. Zhou, W. Wang, B. Liu, Y. Lv, W. Yang, D. Xu, Y. Liu, *J. Alloys Compd.* **2018**, *760*, 15.
[15] L. Peltier, S. Berveiller, F. Meraghni, P. Lohmuller, P. Laheurte, *Shape Memory Superelas.* **2021**, *7*, 194.
[16] W. Jiao, J. Miao, Y. Lu, X. Chen, Z. Ren, G. Yin, T. Li, *J. Alloys Compd.* **2023**, *941*, 168975.
[17] Y. Zou, S. Maiti, W. Steurer, R. Spolenak, *Acta Materialia* **2014**, *65*, 85.
[18] X. Zhang, X. Cui, G. Jin, Y. Qi, Q. Zhang, Q. Ding, M. Qi, *J. Alloys Compd.* **2022**, *925*, 166741.
[19] M. S. Karakaş, A. Günen, C. Çarboğa, Y. Karaca, M. Demir, Y. Altınay, A. Erdoğan, *J. Alloys Compd.* **2021**, *886*, 161222.
[20] P. Moazzen, M. R. Toroghinejad, P. Cavaliere, *J. Alloys Compd.* **2021**, *870*, 159410.
[21] L. Qiao, R. V. Ramanujan, J. Zhu, *Adv. Eng. Mater.* **2023**, *25*, 2300557.
[22] X. An, H. Li, X. Yang, J. Jiang, Z. Liu, L. Kan, L. Zhang, B. Gan, W. Wei, C. Chu, W. Sun, *Adv. Eng. Mater.* **2025**, *27*, 2402102.
[23] J. Wu, Y. Chen, H. Zhu, *Adv. Eng. Mater.* **2022**, *24*, 2101548.
[24] C. Y. Hsu, C. C. Juan, W. R. Wang, T. S. Sheu, J. W. Yeh, S. K. Chen, *Mater. Sci. Eng. A* **2011**, *528*, 3581.
[25] S. Nsoesie, R. Liu, K. Jiang, M. Liang, *Int. J. Mater. Mech. Eng.* **2013**, *2*, 48.
[26] M. Pole, M. Sadeghilaridjani, J. Shittu, A. Ayyagari, S. Mukherjee, *J. Alloys Compd.* **2020**, *843*, 156004.
[27] P. Cui, Y. Liu, F. Zhou, Z. Lai, J. Zhu, *J. Alloys Compd.* **2022**, *903*, 163883.
[28] C. Liang, C. Wang, K. Zhang, H. Tan, M. Liang, Y. Xie, W. Liu, J. Yang, S. Zhou, *J. Alloys Compd.* **2022**, *911*, 165082.
[29] P. Zhao, J. Li, Y. Zhang, X. Li, M. M. Xia, B. G. Yuan, *J. Alloys Compd.* **2021**, *862*, 1.
[30] G. S. Firstov, T. A. Kosorukova, Y. N. Koval, P. A. Verhovlyuk, *Shape Memory and Superelasticity* **2015**, *1*, 400.
[31] Q. Liao, T. Jing, Y. Wang, H. Peng, Y. Wen, *J. Alloys Compd.* **2022**, *926*, 166803.
[32] D. Piorunek, O. Oluwabi, J. Frenzel, A. Kostka, H. J. Maier, C. Somsen, G. Eggeler, *J. Alloys Compd.* **2020**, *857*, 157467.
[33] L. Zhang, T. Hashimoto, J. Yan, *CIRP Ann.* **2021**, *70*, 37.
[34] T. Richter, D. Schroepfer, M. Rhode, A. Boerner, R. S. Neumann, M. Schneider, G. Laplanche, *Mater. Chem. Phys.* **2022**, *275*, 125271.
[35] A. Polishetty, M. M. R. Barla, G. Littlefair, D. Fabijanic, *METMG 2015: Proc. of the Manufacturing Engineering and Technology for Manufacturing Growth 2015 Inter. Conf.* **2015**, pp. 41–45.
[36] T. X. Bui, T. H. Fang, C. I. Lee, *J. Alloys Compd.* **2022**, *924*, 166525.
[37] N. Anbarasan, B. K. Gupta, S. Prakash, P. Muthukumar, R. Oyyaravelu, R. J. F. Kumar, S. Jerome, *Mater. Today: Proc.* **2018**, *5*, 7716.
[38] J. J. Schirra, *Superalloys* **1997**, *718*, 431.
[39] X. You, Y. Tan, S. Shi, J. M. Yang, Y. Wang, J. Li, Q. You, *Mater. Sci. Eng. A* **2017**, *689*, 257.
[40] A. Devillez, G. Le Coz, S. Dominiak, D. Dudzinski, *J. Mater. Proc. Technol.* **2011**, *211*, 1590.
[41] D. Dudzinski, A. Devillez, A. Moufki, D. Larrouquère, V. Zerrouki, J. Vigneau, *Int. J. Mach. Tools Manuf.* **2004**, *44*, 439.
[42] M. C. Troparevsky, J. R. Morris, P. R. C. Kent, A. R. Lupini, G. M. Stocks, *Phys. Rev. X* **2015**, *5*, 1.
[43] X. Yang, Y. Zhang, *Mater. Chem. Phys.* **2012**, *132*, 233.
[44] S. Guo, Q. Hu, C. Ng, C. T. Liu, *Intermetallics* **2013**, *41*, 96.
[45] S. Guo, C. T. Liu, *Prog. Nat. Sci.: Mater. Int.* **2011**, *21*, 433.
[46] J. W. Yeh, *JOM* **2013**, *65*, 1759.
[47] L. Peltier, P. Lohmuller, F. Meraghni, E. Patoor, P. Laheurte, S. Berveiller, *Shape Memory Superelas.* **2022**, *8*, 335.
[48] Z. Dong, A. Sun, S. Yang, X. Yu, H. Yuan, Z. Wang, L. Deng, J. Song, D. Wang, Y. Kang, *Corros. Sci.* **2023**, *220*, 111222.
[49] H. Wu, S. Huang, C. Zhu, H. Zhu, Z. Xie, *Prog. Nat. Sci.: Mater. Int.* **2020**, *30*, 239.
[50] Y. Zhou, D. Zhou, X. Jin, L. Zhang, X. Du, B. Li, *Sci. Rep.* **2018**, *8*, 1.
[51] Y. Zhang, T. T. Zuo, Z. Tang, M. C. Gao, K. A. Dahmen, P. K. Liaw, Z. P. Lu, *Prog. Mater. Sci.* **2014**, *61*, 1.
[52] S. Guo, C. Ng, J. Lu, C. T. Liu, *J. Appl. Phys.* **2011**, *109*, 10.
[53] S. Haas, M. Mosbacher, O. N. Senkov, M. Feuerbacher, J. Freudenberger, S. Gezgin, R. Völkl, U. Glatzel, *Entropy* **2018**, *20*, 1.
[54] J. Yeh, *Recent Prog. High Entr. Alloys* **2006**, *31*, 633.
[55] Y. Zhang, W. J. Peng, *Proc. Eng.* **2012**, *27*, 1169.
[56] Y. Zhang, Y. J. Zhou, J. P. Lin, G. L. Chen, P. K. Liaw, *Adv. Eng. Mater.* **2008**, *10*, 534.
[57] D. B. Miracle, O. N. Senkov, *Acta Mater.* **2017**, *122*, 448.
[58] P. Kumari, A. K. Gupta, R. K. Mishra, M. S. Ahmad, R. R. Shahi, *J. Magn. Magn. Mater.* **2022**, *554*, 169142.
[59] D. J. M. King, S. C. Middleburgh, A. G. McGregor, M. B. Cortie, *Acta Mater.* **2016**, *104*, 172.
[60] L. Liu, Y. Zhang, J. Han, X. Wang, W. Jiang, C. T. Liu, Z. Zhang, P. K. Liaw, *Adv. Sci.* **2021**, *8*, 2100870.
[61] D. Xu, X. Wang, Y. Lu, *Adv. Funct. Mater.* **2024**, *34*, 2408941.
[62] A. Lozinko, R. Gholizadeh, Y. Zhang, U. Klement, N. Tsuji, O.V. Mishin, S. Guo, *Mater. Sci. Eng. A* **2022**, *833*, 142558.
[63] Z. Li, D. Raabe, *JOM* **2017**, *69*, 2099.
[64] A. M. Manzoni, U. Glatzel, *Mater. Charac.* **2019**, *147*, 512.
[65] K. Zhang, Z. Fu, *Intermetallics* **2012**, *22*, 24.
[66] A. Verma, P. Tarate, A. C. Abhyankar, M. R. Mohape, D. S. Gowtam, V. P. Deshmukh, T. Shanmugasundaram, *Scr. Mater.* **2019**, *161*, 28.
[67] S. W. Kim, D. W. Lee, M. C. Kang, J. S. Kim, *J. Mater. Proc. Technol.* **2001**, *111*, 256.
[68] S. Olovsjo, L. Nyborg, *Wear* **2012**, *282*, 12.
[69] S. Sui, H. Tan, J. Chen, C. Zhong, Z. Li, W. Fan, A. Gasser, W. Huang, *Acta Mater.* **2019**, *164*, 413.
[70] A. Strondl, R. Fischer, G. Frommeyer, A. Schneider, *Mater. Sci. Eng. A* **2008**, *480*, 138.
[71] M. Fischer, D. Joguet, G. Robin, L. Peltier, P. Laheurte, *Mater. Sci. Eng. C* **2016**, *62*, 852.
[72] Y. Kaynak, *Int. J. Adv. Manuf. Technol.* **2014**, *72*, 919.
[73] M. Schneider, G. Laplanche, *Acta Mater.* **2021**, *204*, 116470.
[74] G. B. Barbi, *Z. Naturforsch.* **1969**, *24*, 1580.